International Journal of Thermofluids 21 (2024) 100530

Contents lists available at ScienceDirect

International Journal of Thermofluids

journal homepage: www.sciencedirect.com/journal/international-journal-of-thermofluids

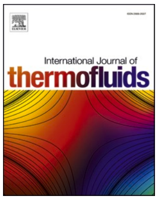

Unsteady magneto-hydrodynamic behavior of TiO_2-kerosene nanofluid flow in wavy octagonal cavity

Tinni Saha [a,b,*], Goutam Saha [c], Nazma Parveen [b], Tarikul Islam [d]

[a] Bangladesh Civil Service, Department of Mathematics, Ministry of Education, Dhaka, Bangladesh
[b] Department of Mathematics, Bangladesh University of Engineering and Technology, Dhaka 1000, Bangladesh
[c] Department of Mathematics, University of Dhaka, Dhaka 1000, Bangladesh
[d] Department of Mathematics, Bangabandhu Sheikh Mujibur Rahman Science & Technology University, Gopalganj, Bangladesh

ARTICLE INFO

Keywords:
TiO_2 nanoparticles
Heat transfer
Kerosene
Spherical shape
Nanofluids

ABSTRACT

The aim of this study is to mathematically model the behavior of magneto-hydrodynamics (MHD) in a two-dimensional unsteady flow, specifically focusing on natural convection (NC) and heat transfer (HT) within a wavy octagonal cavity. The study investigates how heat is transferred and fluid flows within this cavity under specific conditions. In particular, it examines the impact of various parameters, such as the Hartmann number (*Ha*), Rayleigh number (*Ra*), and the volume fraction of nanoparticles (ϕ) on the flow and HT patterns. This cavity includes a rectangular vertical wall (RVW) at the center of its bottom wall, filled with kerosene-TiO_2 nanofluid of spherical shape. Within this setup, the RVW is maintained at a high temperature ($T = T_h$), while the wavy wall is kept at a lower temperature ($T = T_c$, where $T_c < T_h$). All other boundaries of the domain are assumed to be adiabatic. The finite element method (FEM) is employed as the solver for the relevant partial differential equations in numerical simulations. The results show excellent agreement with previously published research papers. The numerical solution transitions from an unsteady state to a steady state in approximately 0.68 dimensionless time units during the HT process. Throughout the study, various parameters are explored, including *Ha*, ranging from 0 to 100, *Ra*, ranging from 10^3 to 10^6, and ϕ, ranging from 0 to 0.05. The findings reveal distinct patterns in streamlines and isotherms. Specifically, a reduction in the rate of HT is observed as the Lorentz force increases, while the rate of HT is enhanced with increasing buoyancy force. Additionally, an expansion in ϕ led to an increase in the rate of HT. The study's findings could contribute to our understanding of fluid dynamics, heat transfer, and the behavior of nanofluids in complex geometries, potentially leading to improvements in various engineering and industrial applications.

1. Introduction

Natural convective (NC) flow of fluid and heat transfer (HT) in various cavities have attracted considerable interest due to their direct applications in engineering disciplines such as geophysical fluid mechanics, solar engineering, nuclear reactor cooling, fire engineering, electrical systems, vehicle cooling systems, and heat exchange in petroleum reservoirs, among others [1]. These systems offer distinct advantages, including reduced noise levels, simplicity, and lower costs.

Abedini et al. [2] investigated MHD-free convective HT in a C-shaped baffled enclosure filled with H_2O–Fe_3O_4 nanofluid, identifying the maximum impact of the baffle on HT at the bottom of the hot wall. The results indicated that the Nusselt number is increased by increasing the enclosure's aspect ratio. Al-Kalbani et al. [3] investigated buoyancy-induced heat transport in a tilted square domain filled with nanofluids. In their numerical simulations, water (H_2O), ethylene glycol (EG), and engine oil (EO) containing Copper (Cu), Aluminium Oxide (Al_2O_3), and Titanium dioxide (TiO_2) nanoparticles were considered. It is found that maximum HT rate is achieved at the critical geometry inclination angle which depends on the concentration of nanoparticles. Al-weheibi et al. [4] investigated numerically natural convective thermal transfer in a trapezoid-shaped enclosure filled with nanoparticles. The study observed that the average Nusselt number (Nu_{avg}) decreased over time until it reached a steady state. Aminossadati and Ghasemi [5] conducted a study on improved NC within a triangular-shaped cavity filled with nanofluids. The findings demonstrated that, in accordance with the modified Maxwell model, HT is generally higher than that

---

[*] Corresponding author at: Bangladesh Civil Service, Department of Mathematics, Ministry of Education, Dhaka, Bangladesh.
E-mail address: tinnisaha4@gmail.com (T. Saha).

https://doi.org/10.1016/j.ijft.2023.100530

Nomenclature

A	dimensionless amplitude of wave
B	dimensionless thickness of rectangular vertical wall
B_0	magnitude of magnetic field [$\mathrm{kgs}^{-2}\mathrm{A}^{-1}$]
C_p	specific heat at constant pressure [$\mathrm{Jkg}^{-1}\mathrm{K}^{-1}$]
Ha	Hartmann number
H	dimensionless length of rectangular vertical wall
g	gravitational acceleration [ms^{-2}]
k	thermal conductivity [$\mathrm{Wm}^{-1}\mathrm{K}^{-1}$]
L	length of cavity [m]
N	dimensionless outward normal vector
D	dimensionless distance of rectangular vertical wall (RVW) from origin
Nu_L	local Nusselt number
Nu_{avg}	mean Nusselt number
Pr	Prandtl number
P	non-dimensional pressure
Ra	Rayleigh number
T	temperature of fluid [K]
U	non-dimensional velocity along x-axis
V	non-dimensional velocity along y-axis
X	non-dimensional x-axis
Y	non-dimensional y-axis
n	shape of nanoparticles

Greek symbols

α	thermal diffusivity [$\mathrm{m}^2\mathrm{s}^{-1}$]
β	thermal expansion coefficient [K^{-1}]
θ	non-dimensional temperature
Δ	dependent dimensionless variable
μ	dynamic viscosity [$\mathrm{kgm}^{-1}\mathrm{s}^{-1}$]
ϕ	solid volume fraction of nanoparticles
τ	dimensionless time
υ	kinematic viscosity [$\mathrm{m}^2\mathrm{s}^{-1}$]
σ	electric conductivity
ρ	density [kgm^{-3}]
λ	non-dimensional period of wave

Subscript

c	cool surface
bf	base fluid
sp	solid particle
h	hot surface
nf	nanofluid

predicted by the original Maxwell model. Arani et al. [6] examined NC in a square cavity filled with nanofluid, consisting of a horizontal heated plate. Their results indicated that $Nu_{avg}$for the vertical walls increased as nanoparticle concentration (ϕ) increased.

Balushi et al. [7] examined free convective HT using magnetic nanoparticles in a square cavity. Their research revealed that nanofluids based on kerosene exhibited a higher HT rate. Hussain and Hussain [8] investigated the enhancement of NC heat transport in a parallelogram-shaped domain that was separately heated and filled with a Cu-H_2O nanofluid. Their results demonstrated a significant increase in HT rate due to the inclusion of the nanoparticles, and they observed that the shape of the convection vortices was influenced by variations in the skew angle. Dogonchi et al. [9] examined NC within a triangular cavity featuring a semicircular bottom wall filled with Cu-H_2O nanofluid. In the absence of a magnetic field, it was noted that a reduction in the radius of the heated semicircle led to an increase in Nu_{avg}. Hwang et al. [10] demonstrated buoyancy-driven HT using H_2O-Al_2O_3 nanofluids within a rectangular domain. Their theoretical findings indicated that the ratio of HT coefficient of nanofluids to that of the base fluid decreased as the average temperature of nanofluids decreased or as the size of nanoparticles increased. Ece and Buyuk [11] conducted a study on MHD NC flow within an inclined rectangular domain with adjacent partitions: cooled and warmed. The results revealed that the temperature fields and flow were significantly affected by the aspect ratio, orientation of the domain, and the direction and strength of the magnetic field.

Ghasemi et al. [12] investigated the impact of magnetic fields on NC within a square-shaped domain filled with nanofluid. Their study revealed that the influence of an increased ϕ on HT performance depended on the values of the Hartmann number (Ha) and Rayleigh number (Ra), leading to either an enhancement or a deterioration. Jou and Tzeng [13] conducted a numerical investigation into the enhancement of natural convective HT within a rectangular domain filled with nanofluids. Their findings indicated that the improvement in HT was contingent upon the parameters ϕ and Ra. Saha et al. [14] explored the characteristics of NC flow and HT within an octagonal cavity, employing various fluids. It is observed that as both Ra and Prandtl number (Pr) increased, there was a corresponding increase in the HT rate. Acharya [15] conducted a thorough investigation into HT characteristics within an octagonal domain filled with Ag-MgO—H_2O hybrid nanofluid (HN). The results indicated that higher Ra and ϕ were positively correlated with increased HT rates, while higher Ha were linked to decreased HT rates. Saboj et al. [16] investigated numerically HT behavior inside an octagonal cavity containing a cool cylinder. Their findings revealed a direct relationship between the HT rate and increasing values of Ra andϕ.

Islam et al. [17] investigated HT behavior in a half-moon-shaped cavity involving both uniform and non-uniform magnetic intensities and temperatures. The study's results indicated that under uniform thermal conditions, HT rate was higher compared to non-uniform heating conditions along the half-moon's diameter. Furthermore, it was observed that a non-uniform magnetic field yielded higher values of Nu_{avg} in comparison to a uniform magnetic field. Islam et al. [18] employed the heatline visualization technique to depict the heat distribution within a prismatic cavity during the process of MHD-free convective heat transport of nanofluid. Their approach, using heatlines, proved more effective in predicting enhanced energy transformation compared to the traditional use of isotherm contours. Uddin et al. [19] conducted numerical simulations to analyze HT within a semi-circular cavity filled with nanofluids, employing a nonhomogeneous dynamic model. Their research revealed that among the various nanofluids examined, CuO—H_2O and Cu-H_2O nanofluids exhibited the most effective performance in enhancing HT rates. Uddin et al. [20] utilized finite element analysis to compute the computational procedure for modeling the convective flow of nanofluids within an annular region. Their findings demonstrated that the annulus with a greater thickness showed higher HT rates. Kalbani and Rahman [21] conducted a study in which they employed a square-shaped inclined cavity filled with nanofluids to investigate HT under the influence of an applied magnetic field and heat source Brownian motion. Their research highlighted that the position of the heat source played a significant role in controlling the HT rates of nanofluids. This study also incorporates a comprehensive examination of the existing research, discussing multiple related studies as cited in references [22–26].

This study identifies several notable research gaps within the existing literature, which provide a foundation for the current investigation. Firstly, there is a notable absence of research on unsteady fluid flow and HT emanating from a heated rectangular vortex generator wing (RVW) within a wavy octagonal cavity, an area that remains largely unexplored. Additionally, there exists a scarcity of detailed studies concerning the influence of nanoparticle shapes on HT, despite the increasing significance of nanofluids in thermal applications. Finally, while the shape of the octagonal cavity has garnered some attention, further research is imperative to determine which geometrical configurations best facilitate efficient thermal transfer processes. Considering this research gap, the primary objective of this numerical analysis is to explore the unsteady MHD natural convection HT and fluid flow phenomena involving nanofluid within a wavy octagonal cavity that includes RVW. This study is motivated by the significant relevance of nanofluids' thermal performance in various engineering processes, such as silver decomposition, heat exchange, crystallization, water evaporation, and more [1]. The research endeavors to contribute to the field by introducing several novel aspects, including a thorough numerical investigation of the impact of magnetic fields, a comprehensive analysis of nanofluid.

2. Physical domain and mathematical modelling

In this study, a mathematical model for the natural convection and heat transfer of nanofluid within an octagonal domain is presented. The flow is assumed to be two-dimensional, incompressible, and time-dependent. A magnetic field exerts its influence in this laminar scenario. The x-axis denotes the dimensional coordinate plane along the base partition, while the *y*-axis is perpendicular to the *x*-axis. The cavity boundaries are assumed to be fixed. A heated RVW at the center of the bottom wall creates a temperature difference, while the wavy top boundary remains cool. The bottom wall, referred to as RVW, is uniformly heated to higher temperature (T_h), while the wavy top boundary is maintained at a lower temperature (T_c). In this scenario, nanoparticles are homogeneously dispersed within the conventional fluid. Thermal slip and thermal equilibrium exist between the nanoparticles and the conventional fluid. It's worth noting that, during convection, the density of nanofluids, which plays a crucial role in buoyancy, varies while other properties remain constant. This is reasonable since the temperature difference is limited between the hot and cold boundaries. Gravity's acceleration opposes the *y*-axis direction, and all solid walls are treated as no-slip boundaries. The geometric setup, along with the coordinate systems, is illustrated in Fig. 1, and the thermo-physical properties of various conventional fluids and nanoparticles are detailed in Table 1.

In this research, the objective is to derive the equations that govern the system in dimensional form, relying on the aforementioned assumptions, as outlined below [22]:

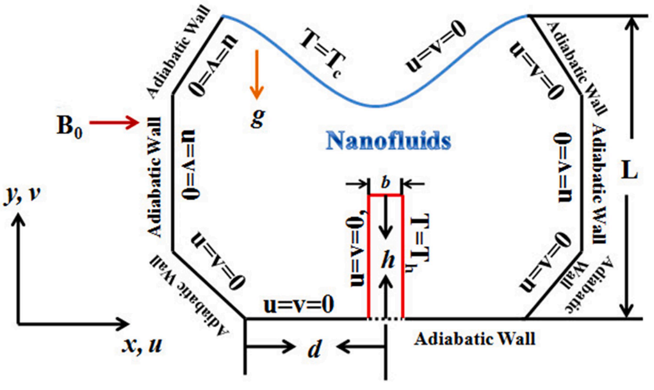

Fig. 1. Schematic diagram of the wavy octagonal domain.

Table 1
Thermophysical Properties of Kerosene and TiO_2.

Base Fluid/ Nanoparticles	c_p [$Jkg^{-1}K^{-1}$]	ρ [kgm^{-3}]	k [$Wm^{-1}K^{-1}$]	$\beta \times 10^{-5}$ [K^{-1}]	σ [Sm^{-1}]
Kerosene	2090	780	0.149	99	6.0×10^{-10}
TiO_2	686.2	4250	8.9538	0.90	2.60×10^{6}

$$\left.\begin{aligned}
&\frac{\partial u}{\partial x}+\frac{\partial v}{\partial y}=0\\
&\rho_{nf}\left(\frac{\partial u}{\partial t}+u\frac{\partial u}{\partial x}+v\frac{\partial v}{\partial y}\right)=-\frac{\partial p}{\partial x}+\mu_{nf}\left(\frac{\partial^2 u}{\partial x^2}+\frac{\partial^2 u}{\partial y^2}\right)\\
&\rho_{nf}\left(\frac{\partial v}{\partial t}+u\frac{\partial v}{\partial x}+v\frac{\partial v}{\partial y}\right)=-\frac{\partial p}{\partial y}+\mu_{nf}\left(\frac{\partial^2 v}{\partial x^2}+\frac{\partial^2 v}{\partial y^2}\right)+(\rho\beta)_{nf}g(T-T_c)-\sigma_{nf}B_0^2 v\\
&(\rho C_p)_{nf}\left(\frac{\partial T}{\partial t}+u\frac{\partial T}{\partial x}+v\frac{\partial T}{\partial y}\right)=\alpha_{nf}\left(\frac{\partial^2 T}{\partial x^2}+\frac{\partial^2 T}{\partial y^2}\right)
\end{aligned}\right\} \tag{1}$$

where *u, v* represents velocities along *x* and *y* directions respectively, *g, p, T* are the gravity, pressure, and temperature respectively, ρ_{nf},μ_{nf}, α_{nf}, $(\rho c_p)_{nf}$, k_{nf}, and $(\rho\beta)_{nf}$ are density, dynamic viscosity, thermal diffusivity, heat capacity, thermal conductivity and volumetric thermal expansion of nanofluid respectively.

2.1. Initial and boundary conditions

$$\begin{aligned}
&\text{For } t>0\\
&\text{Topwall}: x=a\cos 2\pi\lambda_0 x; T=Tc, u=0, v=0\\
&\text{Left and right side walls}:\ u=v=0, \frac{\partial T}{\partial x}=0\\
&\text{Bottom wall}:\ u=v=0, \frac{\partial T}{\partial y}=0\\
&\text{Inclined walls}:\ u=v=0, \frac{\partial T}{\partial n}=0\\
&\text{RVW surfaces}:\ 0\le y\le h;\ x=d+\frac{b}{2}\ \textit{and}\ x=d-\frac{b}{2}\\
&\text{RVW}:\ u=v=0,\ T=T_h
\end{aligned} \tag{2}$$

2.2. Thermophysical properties of nanofluid

The following thermophysical properties of density, viscosity, electrical conductivity, heat capacitance, thermal expansion coefficient, thermal conductivity, and thermal diffusivity are considered [22].

$$\left.\begin{aligned}
&\rho_{nf}=(1-\phi)\rho_{bf}+\phi\rho_{sp}\\
&(\rho c_p)_{nf}=(1-\phi)(\rho c_p)_{bf}+\phi(\rho c_p)_{sp}\\
&(\rho\beta)_{nf}=(1-\phi)(\rho\beta)_{bf}+\phi(\rho\beta)_{sp}\\
&\mu_{nf}=\mu_{bf}\frac{1}{(1-\phi)^{2.5}}\\
&\alpha_{nf}=\frac{k_{nf}}{(\rho c_p)_{nf}}\\
&\frac{k_{nf}}{k_{bf}}=\frac{k_{sp}+(n-1)k_{bf}-(n-1)(k_{bf}-k_{sp})\phi}{k_{sp}+(n-1)k_{bf}+(k_{bf}-k_{sp})\phi}\\
&\sigma_{nf}=\frac{\sigma_{sp}+2\sigma_{bf}-2(\sigma_{bf}-\sigma_{sp})\phi}{\sigma_{sp}+2\sigma_{bf}+(\sigma_{bf}-\sigma_{sp})\phi}\sigma_{bf}
\end{aligned}\right\} \tag{3}$$

In order to convert the governing system (1) and (2) into dimensionless form, following dimensionless variables are introduced [22].

$$\left.\begin{aligned}&X=\frac{x}{L},Y=\frac{y}{L},U=\frac{uL}{\alpha_{bf}},V=\frac{vL}{\alpha_{bf}},\theta=\frac{T-T_c}{T_h-T_c},P=\frac{pL^2}{\rho_{nf}\alpha_{bf}^2},\\&\tau=\frac{t\alpha_{bf}}{L^2},\lambda=\frac{\lambda_0}{L},D=\frac{d}{L},H=\frac{h}{L},A=\frac{a}{L},B=\frac{b}{L}\end{aligned}\right\}\tag{4}$$

Hence the dimensionless system becomes [22]:

$$\left.\begin{aligned}&\frac{\partial U}{\partial X}+\frac{\partial V}{\partial Y}=0\\&\frac{\partial U}{\partial \tau}+U\frac{\partial U}{\partial X}+V\frac{\partial U}{\partial Y}=-\frac{\rho_{bf}}{\rho_{nf}}\frac{\partial P}{\partial X}+\Pr\frac{\mu_{nf}}{\mu_{bf}}\frac{\rho_{bf}}{\rho_{nf}}\left(\frac{\partial^2 U}{\partial X^2}+\frac{\partial^2 U}{\partial Y^2}\right)\\&\frac{\partial V}{\partial \tau}+U\frac{\partial V}{\partial X}+V\frac{\partial V}{\partial Y}=-\frac{\rho_{bf}}{\rho_{nf}}\frac{\partial P}{\partial Y}+\Pr\frac{\mu_{nf}}{\mu_{bf}}\frac{\rho_{bf}}{\rho_{nf}}\left(\frac{\partial^2 V}{\partial X^2}+\frac{\partial^2 V}{\partial Y^2}\right)\\&\qquad+\frac{(\rho\beta)_{nf}}{\rho_{nf}\beta_{bf}}Ra\Pr\theta-\frac{\rho_{bf}}{\rho_{nf}}\frac{\sigma_{nf}}{\sigma_{bf}}Ha^2\Pr V\\&\frac{\partial \theta}{\partial \tau}+U\frac{\partial \theta}{\partial X}+V\frac{\partial \theta}{\partial Y}=\frac{\alpha_{nf}}{\alpha_{bf}}\left(\frac{\partial^2 \theta}{\partial X^2}+\frac{\partial^2 \theta}{\partial Y^2}\right)\end{aligned}\right\}.\tag{5}$$

where, *Ra* is the Rayleigh number, *Pr* is the Prandtl number, and *Ha* is the Hartmann number.

For$\tau>0$

Top wall : $\theta = 0,\ U = 0,\ V = 0$

Left and right side walls : $X = A\cos 2\pi\lambda X;\quad U = 0,\ V = 0,\ \dfrac{\partial\theta}{\partial X}=0$

Bottom wall : $U = 0,\ V = 0,\ \dfrac{\partial\theta}{\partial Y}=0$

Inclined walls : $U = 0,\ V = 0,\ \dfrac{\partial\theta}{\partial N}=0$

RVW surfaces : $0\le Y\le H;\ X=D+\dfrac{B}{2}$ *and* $X=D-\dfrac{B}{2}$

RVW : $U = V = 0,\ \theta = 1$

(6)

Local and average Nusselt number at hot RVW are expressed as [22]:

$$Nu_L=\frac{Lq_w}{k_{bf}(T_h-T_c)},\ \text{where},q_w=-k_{nf}\left(\frac{\partial T}{\partial y}\right)_{y=0}\tag{7a}$$

$$Nu_{avg}=\left(\frac{k_{nf}}{k_{bf}}\right)\int\frac{\partial\theta}{\partial Y}dX\tag{7b}$$

3. Numerical modelling

The governing equations (Eqs. 5) along with the boundary conditions (Eqs. 6) are solved using the Finite Element Method (FEM) in the Galerkin weighted residual (GWR) form, as described in [27]. The convective and diffusive terms are approximated using second-order discretizations, with the utilization of the SIMPLE algorithm for pressure-velocity coupling resolution, along with a Newton-Raphson iteration scheme to solve the resulting nonlinear algebraic equations in a comprehensive computational approach. Convergence of the numerical solution is assessed by monitoring the norm of the difference between consecutive iterations, denoted as $|M^{i+1}-M^i|\le 10^{-5}$,where *M* represents the dependent variables *θ, U*, and *V*, and *i* is the iteration number.

3.1. Grid independence test

A mesh analysis of non-uniform grids was conducted for the grid suitability when$Ra = 10^6$,$Ha = 100$, $Pr = 23.004$, $\phi = 0.05$, $n = 3$, and $\tau = 1$ within the wavy octagonal cavity consisting of a rectangular vertical wall. Five different non-uniform grids were examined, each with a varying number of components: 1589, 1782, 2530, 5820, and 22,414.

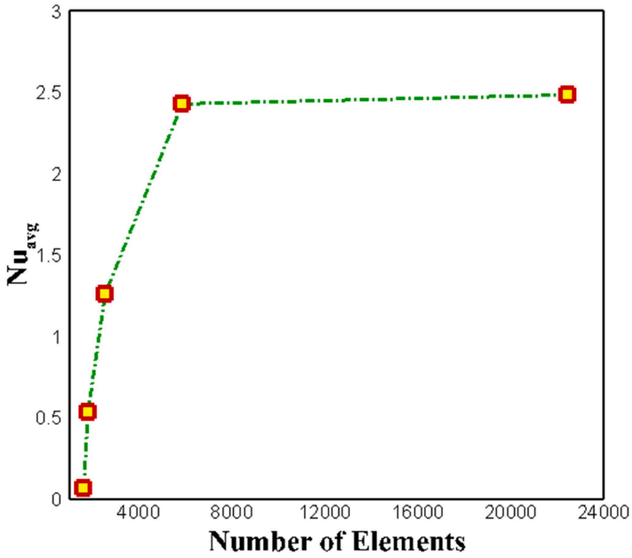

Fig. 2. Mean Nusselt numbers' (Nu_{avg}) convergence for several components number for Kerosene-TiO$_2$ nanofluid when $Ra = 10^6$, $Ha = 100$, $Pr = 23.004$, $n = 3$, $\phi = 0.05$ and $\tau = 1$.

Fig. 2 illustrates the grid refinement process, assessed by numerically calculating Nu_{avg} for the different grid sizes. The comparison between Nu_{avg}at grid sizes 5820 and 22,414 suggests that using elements of these sizes ensures accurate results without errors. For this research, a grid size of 5820 was chosen to ensure grid independence and meet computational time constraints.

3.2. Validation

To enhance the precision of our current numerical method, a comparison was made between the present results and those presented by Saha et al. [14], utilizing streamlines and isothermal profiles at $Pr = 0.71$ as shown in Fig. 3. The findings confirm the reliability of our numerical code and further bolster its credibility for practical applications.

4. Results and discussion

In this study, the numerical analysis investigate the flow phenomena and thermal transport happened in the wavy octagonal shape domain space including RVW. The primary focus of this investigation centers on elucidating HT characteristics of a kerosene-TiO$_2$ nanofluid under varying parameters. These parameters are *Ha* ranging from 0 to 100, *Ra* spanning from 10^3 to 10^6, and ϕ varying from 0 to 5%. The impact of these aforementioned parameters on both fluid flow and temperature distribution will be illustrated using streamline and isothermal contours. Furthermore, this examination explores the comparison between unsteady-state conditions ($\tau = 0.3$) and steady-state conditions ($\tau = 0.7$).

4.1. Variation of Ha

Fig. 4 illustrates streamlines and isotherms under varying *Ha* for both the non-steady case ($\tau = 0.3$) and the steady case ($\tau = 0.7$) with $Ra = 10^5$, $\phi = 0.04$. When $Ha = 0$, the depiction reveals the presence of two symmetric vortices within the cavity adjacent to the RVW boundary. In one of these vortices, fluid flows in a clockwise direction, while in the other, it moves counterclockwise. The strength of this rotational flow diminishes as *Ha* increases. At $Ha = 50$, a comparatively smaller circulation is observed on both sides of the RVW. Near the wavy wall, an additional vortex is noticeable for $\tau = 0.3$, and two additional vortices are evident for $\tau = 0.7$. However, when *Ha* reaches 80, the vortices

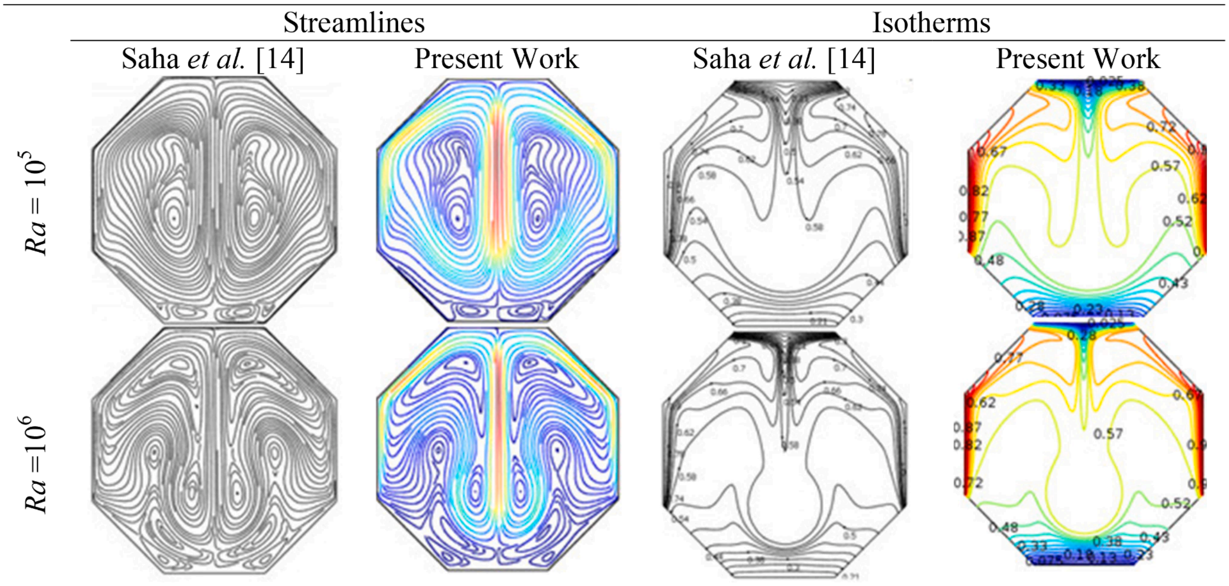

Fig. 3. Variation of streamlines and isotherm profiles of Saha et al. [14] with current results when $Pr = 0.71$.

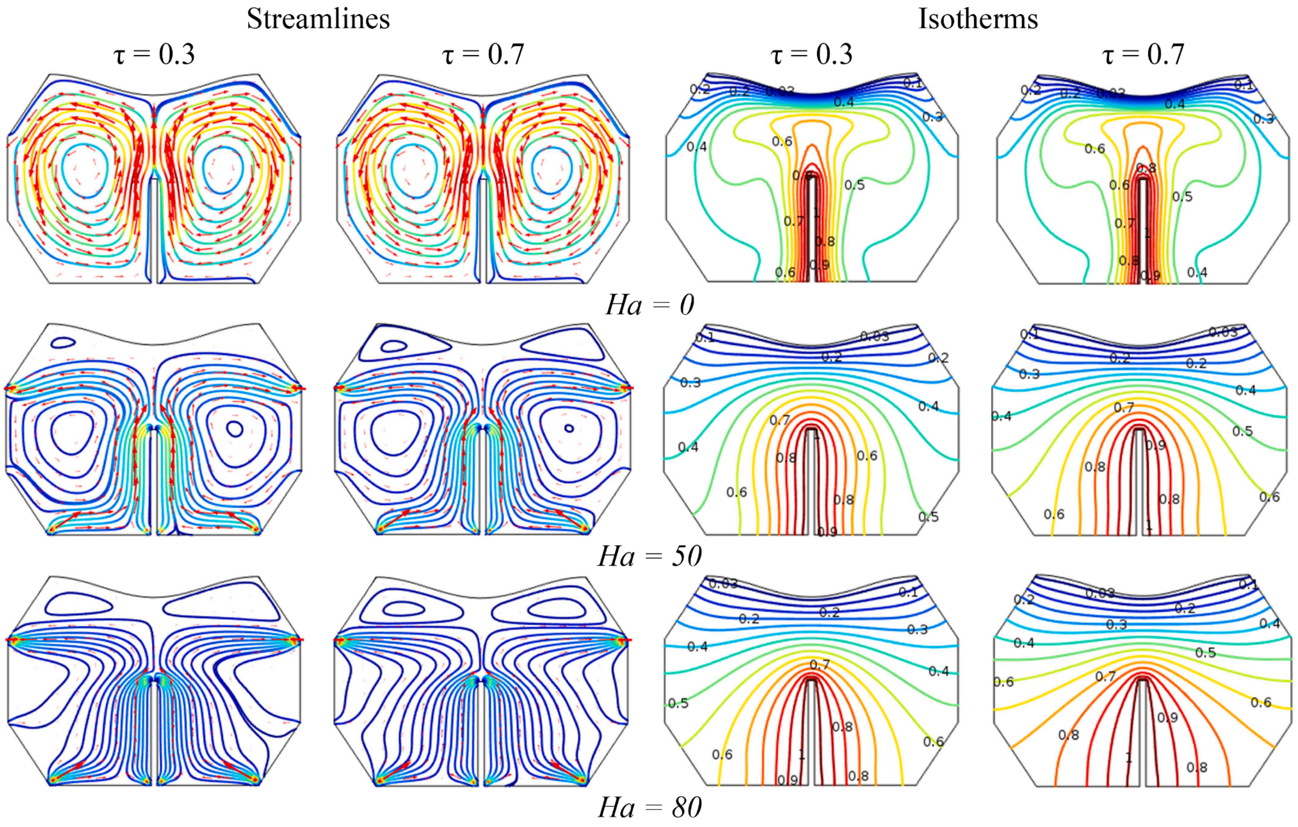

Fig. 4. Variation of Streamline and Isotherms contours at different Ha with $Ra = 10^5$, $\phi = 4\%$ and $n = 3$.

vanish. In this case, the streamlines on both sides of the RVW exhibit no rotation, but two extra vortices emerge near the wavy wall. It is due to the magnetic effect that reduces flow circulation within the domain. Additionally, the Lorentz force generated by the applied magnetic field tends to impede fluid activity, effectively disabling the flows within the domain. Furthermore, as shown in Fig. 4, the contour plots of isotherms are presented for both the unsteady and steady cases. In the steady case, it is evident that the isotherm contours shift and become closer to the hot RVW when $Ha = 0$. However, for higher Ha, such as $Ha = 50$ and 80, the isothermal lines form parabolic shapes around the RVW, gradually aligning themselves with the wavy upper boundary. The spacing between the isothermal lines is more pronounced in proximity to the heated RVW and decreases as Ha increases. This observation suggests the dominance of heat conduction near the warm wall.

4.2. Variation ofϕ

In Figs. 5, the influence of streamline and isothermal contours for

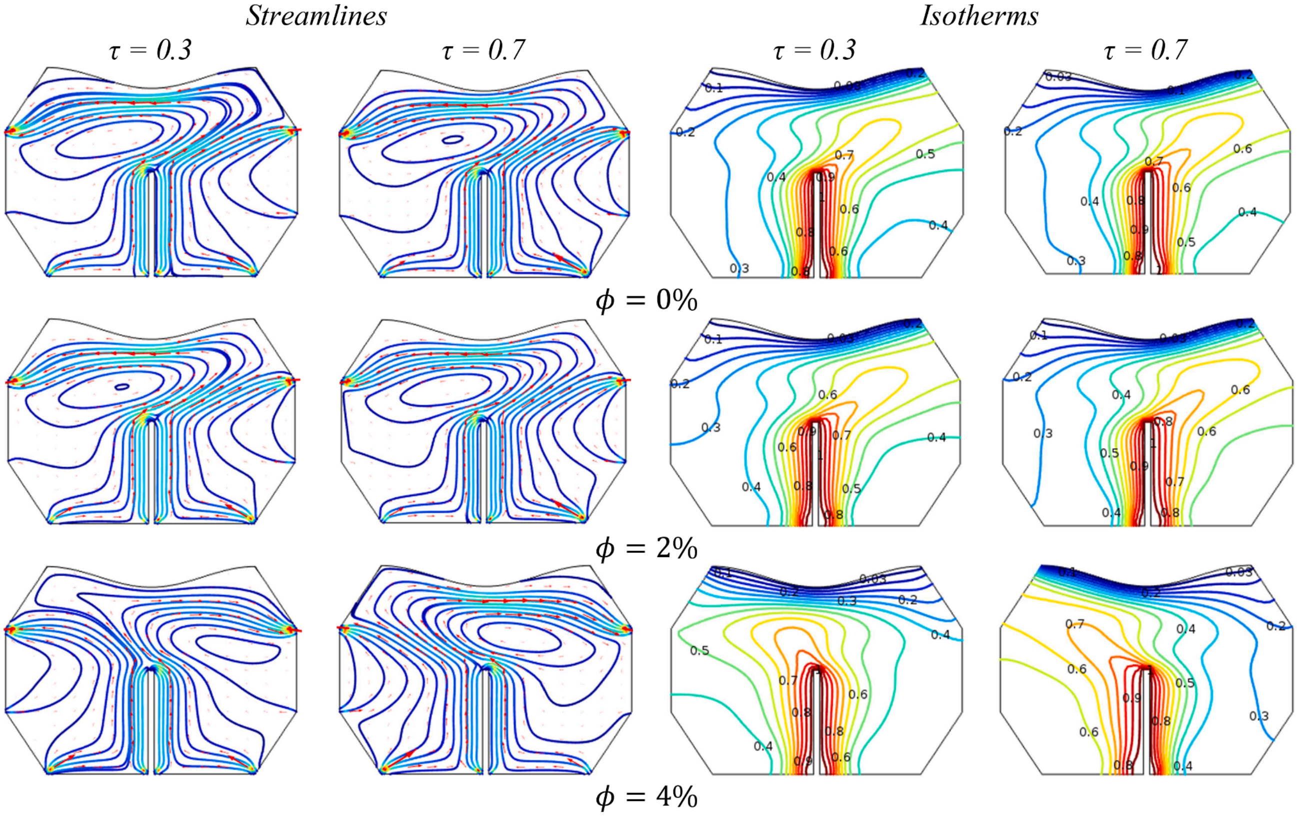

Fig. 5. Variation of Streamline and Isotherms contours at different ϕ with Ra = 10^6, Ha = 80 and n=3.

variousϕ values is examined, with $Ha = 80$ and $Ra = 10^6$, considering both τ = 0.3 (unsteady) and τ = 0.7 (steady) cases. Across both time scales, a consistent pattern emerges: at $\phi = 0\%$, two counter-rotating cells exist within the cavity on opposing sides of RVW, with the left cell being larger and a small vortex forming in its middle under steady conditions. At$\phi = 2\%$, the streamline pattern remains unchanged, but the additional vortex appears during the unsteady state. Conversely, for$\phi = 4\%$, the streamline pattern reverses, with the rightward circulation dominating the left, and slight variations are observed between steady and unsteady cases, influenced by thermal boundary conditions. Notably, the addition of even a small quantity of nanoparticles into the conventional fluid results in decreased streamline functionality. This reduction can be attributed to increase fluid mass, which elevates inertia forces, causing a marginal slowdown in fluid flow, and augmented nanoparticle presence, intensifying particle interactions and viscosity, consequently diminishing the streamline patterns.

Additionally, it is evident that the isotherms closely constrict near the heated RVW. Starting from the head of the warm RVW, the isotherms are notably distorted towards the right side for $\phi = 0\%$, and near the undulating cold upper wall, the isothermal lines run parallel to the upper wall. A slight disparity in the isothermal line patterns is observed between steady and unsteady conditions, with minor alterations noted for$\phi = 2\%$. However, at$\phi = 4\%$, the distortion occurs on the left side in both steady and unsteady states, while all other patterns remain consistent. The dense packing of isotherms suggests that heat conduction is the primary mode of HT. Within the region around the RVW, there is a lower density of isotherms, indicating a higher HT region. Notably, the adjacent fluid particles near the hot RVW move upward after being heated, suggesting convective HT in that particular area.

4.3. Variation of Ra

Figs. 6 presents the impact of Ra ($10^3 \leq Ra \leq 10^6$), on streamlines and isotherms profiles under both unsteady conditions (τ = 0.3) and steady conditions (τ = 0.7), with $\phi = 0.04$, $Ha = 20$. Results reveal that, across all values of Ra, there is clear evidence of buoyancy-induced rotating flows within the cavity. In both unsteady (τ = 0.3) and steady (τ = 0.7) scenarios, two symmetric circular flow patterns are observed on either side of the RVW within the cavity for $Ra = 10^3$. Additionally, for τ = 0.7, two extra vortices emerge near the wavy cold upper wall, although they diminish in intensity for $Ra = 10^4$. The rotational cells exhibit increased strength for $Ra = 10^5$. In all three cases, the flow direction of one rotating cell is clockwise, while the other is counterclockwise. However, for $Ra = 10^6$, a significant change in the flow pattern is noted. Under τ = 0.3, two differently oriented rotating cells are observed, distinct from the $Ra = 10^5$ scenario. Specifically, there is one relatively large rotating cell observed on the right-hand side of the RVW, and a compressed cell is seen on the left side under steady time (τ = 0.7).

Isothermal profiles are also presented in Fig. 6. At $Ra = 10^3$, the isotherm patterns display a pronounced curvature around the RVW and gradually approach near-parallel alignment with the wavy cold boundary within the domain, indicating weak convection. Near the heated RVW, the isothermal lines take on a parabolic shape, and they tend to align almost parallel to the adjacent cool wavy upper boundary. As Ra increases, signifying higher Ra, the fluid currents gain strength due to the intensified buoyancy effects, and the isothermal patterns start to deform more around the hot RVW. This suggests the onset of convection, with convection becoming the dominant mode of HT within the domain. At $Ra = 10^5$, characterized by a high Ra, the isotherms adopt a distinctive mushroom-like configuration. This specific isothermal contour style indicates that heat energy is flowing into the nanofluid from the heated RVW within the domain. As Ra further increases to 10^6, corresponding to an even higher Ra, the isothermal lines deviate from the mushroom shape, indicating further complex changes in heat transfer patterns.

Fig. 7 illustrates the variation of Nu_{avg} for a bottom-heated RVW at $Ra = 10^6$, $n = 3$, and $\phi = 0.05$, plotted against non-dimensional time (τ)

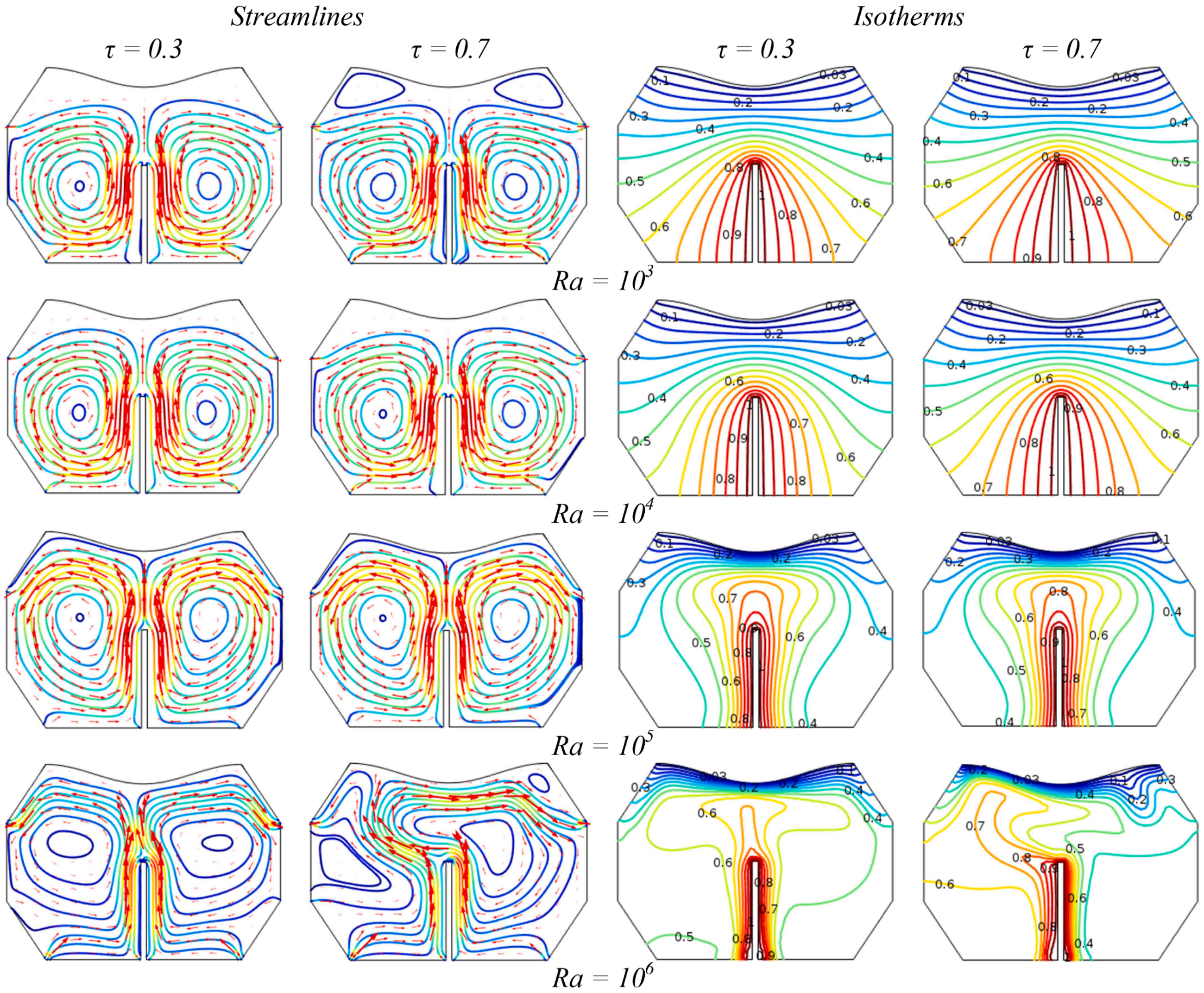

Fig. 6. Variation of Streamline and Isotherms contours at different Ra with ϕ = 4%, Ha = 20.

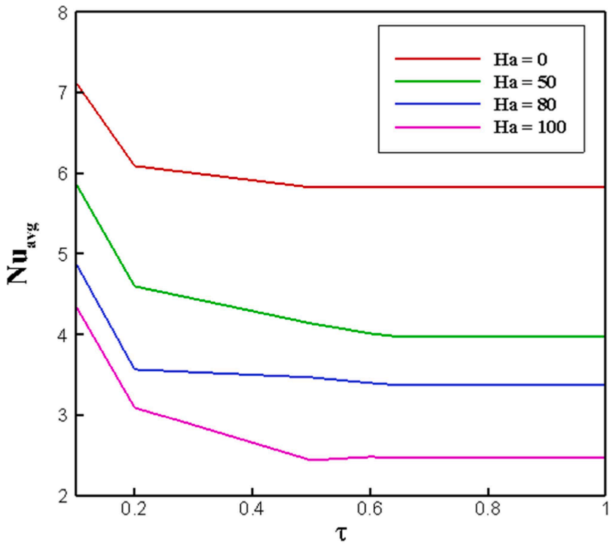

Fig. 7. Variation of Nu_{avg} with different Ha for ϕ = 0.05, $Ra = 10^6$ and n = 3.

for different values of Ha. The plots reveal a significant initial decrease in Nu_{avg} for various Ha values. However, after a certain period, Nu_{avg} stabilizes, indicating the system reaches a steady-state with respect to Ha. Fig. 7 clearly demonstrates that Nu_{avg} decreases as Ha increases, and this decrease is more pronounced for lower magnetic influence. On the other hand, when the magnetic field intensity is higher, the rate of Nu_{avg} reduction is comparatively lower.

Fig. 8 illustrates the impact of varying ϕ on Nu_{avg} in a bottom-heated RVW with different dimensionless time values. This analysis is conducted under the conditions of $Ra = 10^6$, $n = 3$, and $Ha = 100$. The visual representation indicates an initial decline in Nu_{avg}, followed by its stabilization after a certain period of time. Moreover, these visualizations clearly demonstrate that the introduction of nanoparticles into the base fluid leads to a significant enhancement of Nu_{avg}. At the onset of the unstable flow, Nu_{avg} is notably higher, but as dimensionless time progresses, it reaches a constant value. Moreover, as the value of ϕ increases, Nu_{avg} exhibits a corresponding increase in values. This suggests that a higher ϕ value is associated with enhanced HT characteristics in the system, indicating a positive correlation between ϕ and Nu_{avg}.

Fig. 9 displays the dynamic changes in Nu_{avg} within a heated RVW configuration for Ha = 100, ϕ = 0.05 and n = 3. This depiction encompasses various Ra ($10^3 \leq Ra \leq 10^6$) plotted against non-dimensional time (τ). These visual representations distinctly illustrate the temporal evolution of Nu_{avg}, transitioning from an unsteady phase to a stable state within the heated RVW. Notably, as Ra increases, Nu_{avg} tends to be

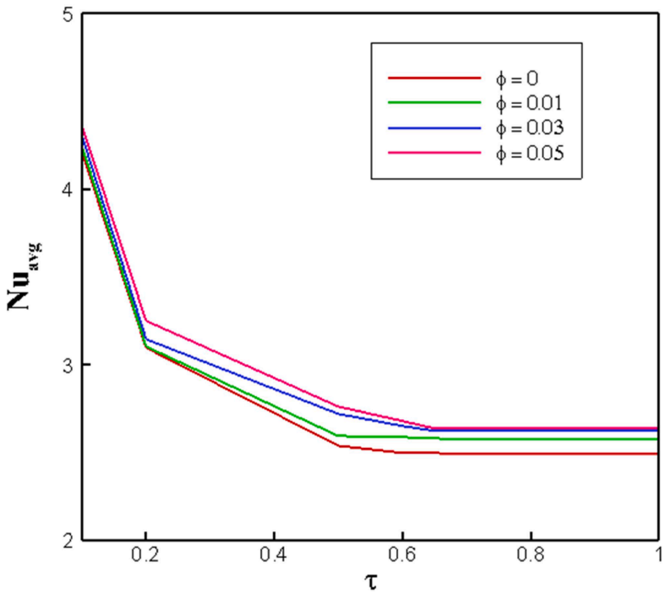

Fig. 8. Variation of Nu_{avg} with different ϕ for $Ha = 100$, $Ra = 10^6$ and n=3.

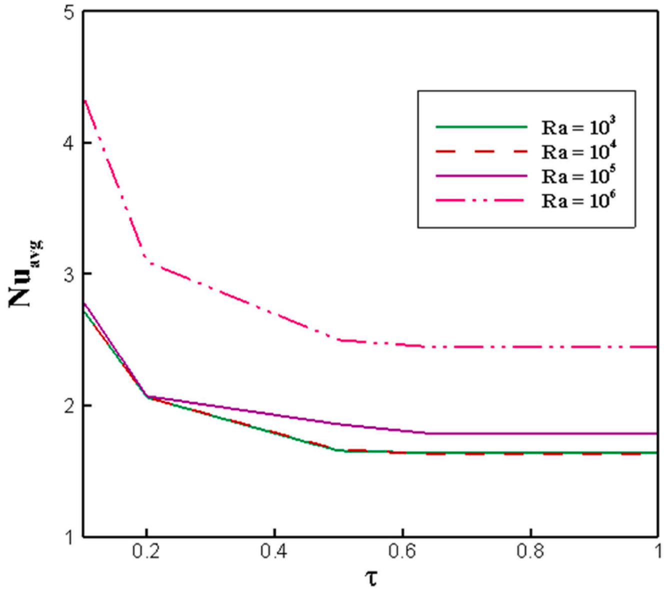

Fig. 9. Variation of Nu_{avg} with different Ra for $Ha = 100$, $\phi = 0.05$ and $n = 3$.

higher along the lower RVW surface. As time progresses, Nu_{avg} gradually converges towards a stable equilibrium, reaching this state after a specific time interval. Specifically, for $Ra = 10^3$ and 10^4, Nu_{avg} is at its lowest point, and as Ra escalates, Nu_{avg} experiences an enhancement due to the increased buoyancy effect.

5. Conclusion

This study examined the MHD natural convection flow of kerosene-TiO_2 nanofluid and heat transfer within a wavy octagonal cavity equipped with a heated rectangular vortex generator wing, where parameters such as *Ra, Ha*, and ϕ vary under uniform thermal boundary conditions. The significant findings are summarized as follows:

- The presence of a magnetic field reduced the flow circulation inside the domain.
- Increased fluid mass slows flow and augmented nanoparticles raise viscosity, reducing streamline patterns.
- The dominance of heat conduction is observed near the heated wall for higher *Ha* values.
- The isothermal contour showed heat flowing into the nanofluid from the heated RVW for different *Ra*.
- With an elevated *Ha*, there is a reduction in the heat transfer rate.
- An augmented concentration of nanoparticles leads to an elevation in the heat transfer rate.
- The heat transfer rate experiences an upsurge as the Rayleigh number increases.

Declaration of Competing Interest

The authors declare that they have no known competing financial interests or personal relationships that could have appeared to influence the work reported in this paper.

Data availability

Data will be made available on request.

References

[1] M. Zafar, H. Sakidin, M. Sheremet, I. Dzulkarnain, R.M. Nazar, A. Hussain, Z. Said, F. Afzal, A. Al-Yaari, M.S. Khan, J.A. Khan, The impact of cavities in different thermal applications of nanofluids: a review, Nanomaterials 13 (6) (2023) 1131. Basel.

[2] A. Abedini, T. Armaghani, A.J. Chamkha, MHD free convection heat transfer of a water–Fe_3O_4 nanofluid in a baffled C-shaped enclosure, J. Therm. Anal. Calorim. 135 (2019) 685–695.

[3] K.S. Al-Kalbani, M.M. Rahman, M.S. Alam, N. Al-Salti, I.A. Eltayeb, Buoyancy induced heat transfer flow inside a tilted square enclosure filled with nanofluids in the presence of oriented magnetic field, Heat Transf. Eng. 39 (6) (2018) 511–525.

[4] S.M. Al-weheibi, M.M. Rahman, M.S. Alam, K. Vajravelu, Numerical simulation of natural convection heat transfer in a trapezoidal enclosure filled with nanoparticles, Int. J. Mech. Sci. 131-132 (2017) 599–612.

[5] S.M. Aminossadati, B. Ghasemi, Enhanced natural convection in an isosceles triangular enclosure filled with a nanofluids, Comput. Math. Appl. 61 (2011) 1739–1753.

[6] A. Arani, M. Mahmoodi, M. Amini, Free convection in a nanofluid filled square cavity with horizontal heated plate, Defect Diffus. Forum 312–315 (2011) 433–438.

[7] L.M.A. Balushi, M.J. Uddin, M.M. Rahman, Natural convective heat transfer in a square enclosure utilizing magnetic nanoparticles, Propuls. Power Res. 8 (3) (2019) 194–209.

[8] S.H. Hussain, A.K. Hussain, Natural convection heat transfer enhancement in a differentially heated parallelogrammic enclosure filled with Cu-water nanofluid, ASME J. Heat Transf. 136 (2014) 82502–82508.

[9] A.S. Dogonchi, M.A. Ismael, A.J. Chamkha, D. D.Ganji, Numerical analysis of natural convection of Cu–water nanofluid filling triangular cavity with semicircular bottom wall, J. Therm. Anal. Calorim. 135 (2019) 3485–3497.

[10] K. Hwang, J. Lee, J. Jang, Buoyancy-driven heat transfer of water-based Al2O3 nanofluids in a rectangular cavity, Int. J. Heat Mass Transf. 50 (2007) 4003–4010.

[11] M.C. Ece, E. Buyuk, Natural convection flow under a magnetic field in an inclined rectangular enclosure heated and cooled on adjacent wall, Fluid Dyn. Res. 38 (2005) 564–590.

[12] B. Ghasemi, S.M. Aminossadati, A. Raisi, Magnetic field effects on natural convection in a nanofluid-filled square enclosure, Int. J. Therm. Sci. 50 (2011) 1748–1756.

[13] R. Jou, S. Tzeng, Numerical research of nature convective heat transfer enhancement filled with nanofluids in rectangular enclosures, Int. Commun. Heat Mass Transf. 33 (6) (2006) 727–736.

[14] G. Saha, S. Saha, M.N. Hasan, M.Q. Islam, Natural convection heat transfer within octagonal enclosure, IJE Trans. A Basics 23 (1) (2010) 1–10.

[15] N. Acharya, On the hydrothermal behavior and entropy analysis of buoyancy driven magnetohydrodynamic hybrid nanofluid flow within an octagonal enclosure fitted with fins: application to thermal energy storage, J. Energy Storage 53 (2022), 105198.

[16] J.H. Saboj, P. Nag, G. Saha, S.C. Saha, Entropy production analysis in an octagonal cavity with an inner cold cylinder: a thermodynamic aspect, Energies 16 (14) (2023) 5487.

[17] T. Islam, N. Parveen, R. Nasrin, Mathematical modeling of unsteady flow with uniform/non-uniform temperature & magnetic intensity in a half-moon shaped domain, Heliyon 8 (3) (2022) e09015.

[18] T. Islam, M.N. Alam, M.I. Asjad, N. Parveen, Y.M. Chu, Heatline visualization of MHD natural convection heat transfer of nanofluid in a prismatic enclosure, Sci. Rep. 11 (2021) 10972.

[19] M.J. Uddin, M.M. Rahman, Numerical computation of natural convective heat transport within nanofluids filled semi-circular shaped enclose using nonhomogenous dynamic model, Tharm. Sci. Eng. Prog. 1 (2017) 25–38.

[20] M.J. Uddin, M.M. Rahman, Finite element computational procedure for convective flow of nanofluids in an annulus, Therm. Sci. Eng. Prog. 6 (2018) 251–267.

[21] A.K. S.Kalbani, M.M. Rahman, Convective heat transfer in nanofluids inside an inclined square enclosure in the presence of heat source Brownian motion and oriented magnetic field, J. Eng. Phys. Thermophys. 92 (5) (2019) 2188–2207.

[22] T. Saha, T. Islam, S. Yeasmin, N. Parveen, Thermal influence of heated fin on MHD natural convection flow of nanofluids inside a wavy square cavity, Int. J. Thermofluids 18 (2023), 100338.

[23] G. Saha, A.A.Y. Al-Waaly, M.C. Paul, S.C. Saha, Heat transfer in cavities: configurative systematic review, Energies 16 (5) (2023) 2338.

[24] M.M. Ikram, G. Saha, S.C. Saha, Unsteady conjugate heat transfer characteristics in hexagonal cavity equipped with a multi-blade dynamic modulator, Int. J. Heat Mass Transf. 200C (2023), 123527.

[25] M.M. Ikram, G. Saha, S.C. Saha, Conjugate forced convection transient flow and heat transfer analysis in a hexagonal, partitioned, air-filled cavity with dynamic modulator, Int. J. Heat Mass Transf. 167 (2021), 120786.

[26] M.A. Taher, S. Siddiqa, M. Kamrujjaman, M.M. Molla, Free convection of temperature-dependent thermal conductivity based ethylene glycol-Al_2O_3 nanofluid in an open cavity with wall heat flux, Int. Commun. Heat Mass Transf. 138 (2022), 106379.

[27] O.C. Zienkiewicz, R.L. Taylor, The Finite Element Method Solid and Structural Mechanics, 6th Edition, McGraw-Hill, 2005.